



Electrodeposition of ZnO thin films on conducting flexible substrates

Filipe F. Oliveira¹, Mariana P. Proenca^{1,*} , João P. Araújo¹, and João Ventura^{1,*} 

¹Departamento de Física e Astronomia, Faculdade de Ciências, IFIMUP and IN-Institute of Nanoscience and Nanotechnology, Universidade do Porto, Rua do Campo Alegre 687, 4169-007 Porto, Portugal

Received: 20 October 2015

Accepted: 20 February 2016

Published online:

8 March 2016

© Springer Science+Business Media New York 2016

ABSTRACT

In this work, we studied the DC electrochemical deposition of zinc oxide (ZnO) thin films on a conducting and flexible substrate, for their application in energy harvesting piezoelectric nanodevices. The deposition process was performed by varying the zinc nitrate concentration (c) in the electrolyte, its temperature (T), and the applied deposition potential (V), and subsequently tracing the influence of such parameters on the morphology (analyzed by scanning electron microscopy), crystallography (X-ray diffraction), and thickness (using the deposition current transient curves) of the ZnO thin films. The variation of the electrodeposition parameters led to the formation of different micro- and nano-structures, such as flat layers, *microflowers*, *nanospheres*, *webs*, and *microramifications*. Furthermore, the analysis of the deposited charge (by integrating the deposition current transients) illustrated an increase in the deposition rate with the increase of T and c , and a decrease of V . Finally, the maximum ZnO film thickness ($\sim 5 \mu\text{m}$) was obtained for $T = 80 \text{ }^\circ\text{C}$, $c = 0.1 \text{ M}$, and $V = -1.5 \text{ V}$. This study provides us important tools to tune the electrochemical growth of ZnO thin films.

Introduction

During the last two decades, great advances have been made in nanofabrication and nanotechnology, which led the production of integrated electronics and microprocessors, to a worldwide practice and propelled their integration in a large range of equipments and technologies. While functional systems and corresponding components become smaller due to research and development, the electric sources required for their proper functioning are still based on temporary storages such as batteries and

capacitors. This is where nanogenerators come into play [1–4]. In a world where integrated circuits are used daily in our smartphones, personal computers, security systems, or sensors, the dream of self-powered devices directly generating electricity from the environment is finally within our grasp. Piezoelectric nanogenerators are one of the most promising devices as they have the ability of harvesting energy from a wide range of sources. Piezoelectric materials, such as barium titanate (BaTiO_3), lead titanate (PbTiO_3), lead zirconium titanate (PZT; $\text{Pb Zr}_x\text{Ti}_{1-x}\text{O}_3$), or zinc oxide (ZnO), allow the conversion of mechanical

Address correspondence to E-mail: marianaproenca@gmail.com; jventura@fc.up.pt

energy, in forms of oscillation, vibration, contact pressure, or bending, into electricity [5].

Zinc oxide (ZnO) is a semiconductor with a wide band gap of 3.3 eV [6]. It usually presents a wurtzite crystalline structure belonging to the $P6_3mc$ space group, which results in a non-centrosymmetric structure and the appearance of piezoelectricity. To maximize this effect, ZnO must have a preferential growth along the [002] crystallographic plane [7]. ZnO also possesses a relatively high coupling coefficient, making it excellent for a wide range of piezoelectric applications, especially when nanostructured [8]. In particular, by tuning the morphology of ZnO nanostructures, one can enhance the efficiency of future devices [8–10]. ZnO can be deposited in thin films or grown in various nanostructure forms [11, 12], such as nanowires, nanotubes, nanorings, or nanobelts, using a wide range of techniques like electrochemical deposition [13–17], chemical vapor deposition (CVD), magnetron sputtering, pulsed laser deposition (PLD), thermal evaporation [18], atomic layer deposition (ALD) [19], spin-coated sol-gel [20–23], vapor liquid solid (VLS) [1, 24], sol-chemical process [25], or hydrothermal growth [5, 26–29]. Among these, the electrochemical deposition is one of the most promising bottom-up nanofabrication approaches due to its simple apparatus, low cost execution, and high control over the geometrical dimensions of the fabricated nanostructures.

In this work, we study the potentiostatic electrochemical deposition of ZnO thin films with tunable thicknesses and morphologies. The influence of the electrolyte concentration, temperature, and applied potential during the deposition process is addressed. Depositions were made on top of flexible polyethylene terephthalate (PET) substrates with a conducting indium tin oxide (ITO) layer, for the fabrication of piezoelectric ZnO thin films with a preferential crystallographic structure.

Experimental procedure

ZnO thin films were electrodeposited in conducting substrates (PET with ITO) using an aqueous solution of zinc nitrate hexahydrate (ZNH) as electrolyte. To better understand the electrodeposition process of ZnO thin films, we studied the influence of three different parameters on the deposited films (Table 1): the concentration of ZNH on the electrolyte, 0.1 and 0.01 M;

Table 1 Parameters varied during the electrochemical deposition process: temperature (RT and 80 °C), concentration of ZNH (0.1 and 0.01 M), and applied potential (−1.0, −1.1, and −1.5 V vs. Ag/AgCl)

Temperature	Concentration					
	0.1 M			0.01 M		
RT (V)	−1.0	−1.1	−1.5	−1.0	−1.1	−1.5
80 °C (V)	−1.0	−1.1	−1.5	−1.0	−1.1	−1.5

the electrolyte temperature, room temperature (RT; ~19 °C) and 80 °C; and the applied deposition potential, −1.0, −1.1, and −1.5 V vs. Ag/AgCl [30].

The potentiostatic electrodepositions were performed in a standard electrochemical cell with a three-electrode system [31]: a Pt mesh as counter electrode, a PET/ITO substrate as working electrode, and a reference electrode of Ag/AgCl (in 4 M KCl) (Fig. 1a). For the electrodepositions at 80 °C (Fig. 1b), we added a hot plate that heats a water bath with the previous set-up inside, magnetic stirring to homogenize the electrolyte temperature, and an extra sealing lid on top to prevent the loss of the electrolyte through evaporation. All depositions lasted 1 h and were performed in substrates with $0.5 \times 1.4 \text{ cm}^2$. Scanning electron microscopy (SEM) images of the samples' surfaces were obtained with high resolution FEI Quanta 400FEG. The chemical composition of the samples was analyzed by energy dispersive X-ray spectroscopy (EDS). The X-ray diffraction (XRD) technique was performed using a Siemens D5000 diffractometer on representative samples and compared to a reference spectrum of the substrate. To estimate the film thickness of the obtained samples, the total charge deposited was analyzed by integrating the deposition current transients.

Results and discussion

Deposition current transients

The monitorization of the current transients $[i(t)]$ during the electrodeposition process allows one to better understand the mechanism of ZnO formation. Figure 2 shows the current transients during the electrodeposition process of selected ZnO thin films on PET substrates with an ITO coating. From the obtained results, we observe an increase of the deposition current with decreasing potential, at room

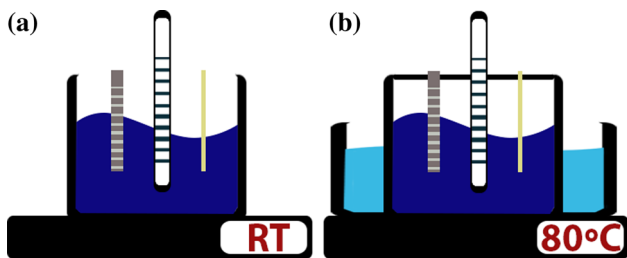


Figure 1 Schematic representation of the electrochemical deposition experimental setup at **a** room temperature and **b** 80 °C, illustrating, from left to right, the counter, reference, and working electrodes, respectively.

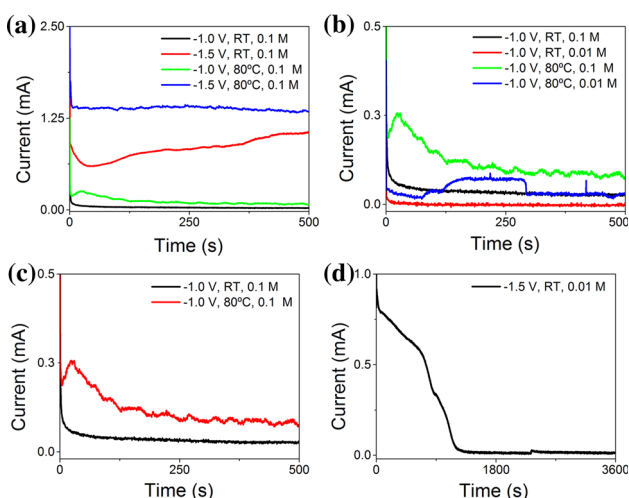


Figure 2 Deposition current transients recorded during the electrodeposition process of selected ZnO thin films electrodeposited at **a** 0.1 M (with different temperatures and applied potentials) and **b** –1.0 V (with different temperatures and concentrations). **c** Comparison plot of representative electrodeposited samples at 0.1 M and –1.0 V, with varying electrolyte temperatures. **d** Complete $i(t)$ current curve for a sample electrodeposited at room temperature with 0.01 M of ZNH under –1.5 V. Note the different time scales.

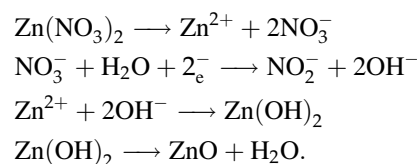
temperature and 80 °C (Fig. 2a). Also, an increase in the deposition current is verified when increasing the solution concentration (Fig. 2b). Finally, comparing representative electrodeposited samples at RT and 80 °C (Fig. 2c), we see that the deposition current also increases with the heated electrolyte. The process is temperature-assisted and thus the heating of the electrolyte increases the deposition rate (seen as an increase in the measured current). Nevertheless, small irregularities occur in the current transients of the heated samples due to the use of magnetic stirring and the existence of convection currents. Note

also that the small differences found in the current transients may come from the lower surface conductivity and the different growth mechanisms observed by SEM, which affect the morphology of the ZnO deposits and consequently the deposition area.

Figure 2d shows the complete curve of the deposition process for a solution with 0.01 M of ZNH, at room temperature and under –1.5 V. Two characteristic zones can be defined in the curve, representing two different deposition behaviors. During the first 1250 s of deposition, the current exhibits high values that progressively decrease until a minimum is reached. This is then followed by the second region of the process, where the current remains constant in its minimum value. This effect will be addressed at the end of “Morphology: deposition at room temperature” section when analyzing the distinct surface morphologies deposited during each stage.

Deposited charge

When the electrodeposition efficiency is of 100 %, which means that all the measured current is used in the electrodeposition process, one can estimate the deposited charge (Q) by integrating the current transient curve ($Q = \int idt$). In this case, we assume that all measured current is used to deposit the Zn^{2+} ions and neglect the current used in any side chemical reactions. The chemical reactions taking place at the substrate (PET with ITO) during ZnO electrodeposition are as follows [32]:



Using the standard size of the PET/ITO substrates ($0.5 \times 1.4 \text{ cm}^2$), we estimated the deposited charge density for all prepared samples (Fig. 3). We can verify that the charge density increases rather linearly over time, during the first 500 s of deposition, showing a constant deposition rate without major changes in the deposition process (Fig. 3a, b). The charge density slopes are also seen to increase with the ZNH concentration and with decreasing applied potential. However, for the values studied in this work, the variation of the deposition potential (from –1.0 and –1.1 to –1.5 V) was found to have a higher influence on the deposited charge values than

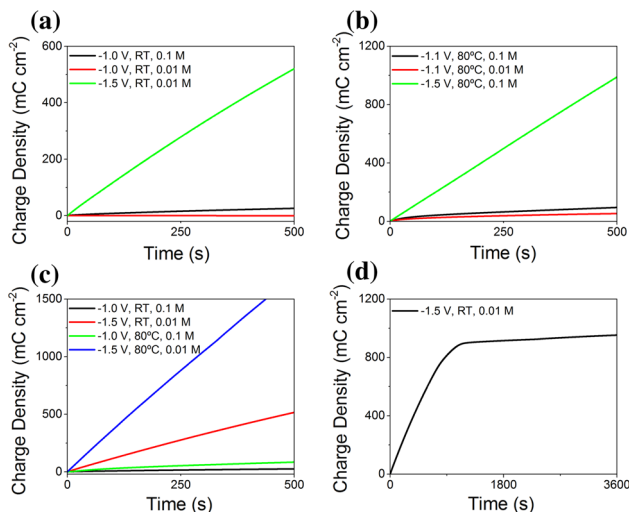


Figure 3 Time dependence of the electrodeposition charge density during the growth of representative ZnO thin films, illustrating the effect of increasing ZNH concentration and applied potential at **a** room temperature and **b** 80 °C. **c** Electrodeposition charge density plots comparing representative electrodeposited samples with varying electrolyte temperature, concentration, and applied potential. **d** Charge density transient curve for the sample electrodeposited at room temperature with 0.01 M of ZNH and under -1.5 V. Note the different time scales.

varying the concentration of ZNH (from 0.01 to 0.1 M). Figure 3a, b clearly shows that lowering the cathodic potential to more negative values produces a faster increase in the deposited charge than increasing the concentration.

Figure 3c compares the deposited charge density plots of representative electrodeposited samples at room temperature and 80 °C. These show that the deposited charge also increases by heating the electrolyte, achieving its maximum value at 80 °C under the larger negative applied potential of -1.5 V. Also, we can again verify that the applied deposition potential produces larger variations of charge density than all the other parameters. For example, the charge density at the larger negative potentials of -1.5 V, combined with the lowest concentration (0.01 M) and temperature (RT) conditions, is still higher than that at the smallest negative potential of -1.0 V, even with the highest and optimized concentration (0.1 M) and temperature (80 °C) conditions (Fig. 3c).

Finally, we can analyze Fig. 3d, where the complete charge density curve of the sample electrodeposited at -1.5 V, with 0.01 M of ZNH and at RT is

shown. As in Fig. 2d, which represents the current transients during the deposition process, this curve can also be divided into two distinct behaviors. The first region, lasting for about 1000 s, shows a linear behavior, similar to other graphs, in which the deposited charge is monotonously increasing. In the second region, from around 1000 s until 3600 s, a linear charge deposition with a much lower slope (almost constant charge density) is observed.

Film thickness

The total deposited charge calculated by integration of the current transient curves allowed us to estimate the total mass of ZnO deposited, using Faraday's laws of electrolysis [33, 34]:

$$m = \frac{QM}{nF},$$

where m is the deposited mass in grams (g), M is the molar density of the deposited material (81.40 g mol⁻¹ for ZnO), Q is the deposited charge in coulombs (C), n is the electronegativity of the deposited ions ($n = 2$ for Zn²⁺), and F is Faraday's constant ($F = 96485$ C mol⁻¹). Knowing the volumetric density of ZnO ($\rho = 5.61$ g cm⁻³) and the deposition area ($A = 0.7$ cm²), one can estimate the thin film's thickness (h) through:

$$h = \frac{m}{A \cdot \rho}.$$

The results are plotted in Fig. 4, where we can see that the highest thickness was obtained at the largest negative applied potential of -1.5 V and at the highest temperature of 80 °C, as expected from the deposited charge transient curves plotted in Fig. 3. At these high values of applied potential and temperature, the deposition process occurs under charge-transfer control [35], in which the concentration of ZNH in the electrolyte becomes negligible. On the other hand, at room temperature, the highest thickness is again obtained at the largest negative potential of -1.5 V, but using the highest concentration of 0.1 M. At this lower temperature, the applied potential is no longer high enough to limit the deposition growth, and this becomes a diffusion-controlled process, which is limited by the mass transport to the samples surface [35]. Therefore, the thickness of the electrodeposited ZnO films at room temperature and at -1.5 V will still depend on the

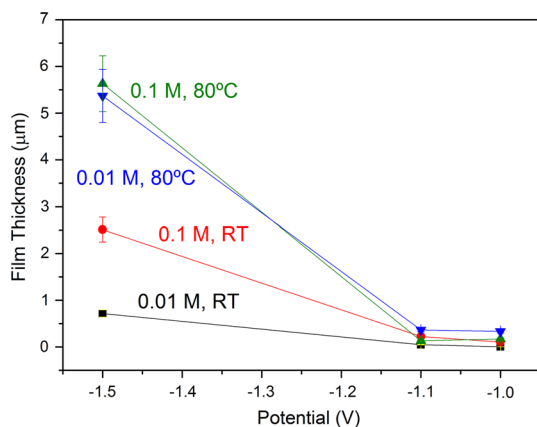


Figure 4 Estimated thickness of the ZnO thin films electrodeposited at different temperatures, concentrations, and applied potentials.

concentration of ZNH in the electrolyte solution, becoming higher at larger concentrations.

Finally, we verify that the estimated thickness tends to increase with the modulus of the applied potential. However, a sudden increase is seen from -1.1 to -1.5 V, which may indicate an unstable deposition at more negative potentials. This effect was also evidenced by the distinct current transients and inhomogeneous morphologies found for the samples deposited at -1.5 V. In the estimated thickness of the electrodeposited thin films, a linear dependency with the applied potential was expected. Nonetheless, the sudden increase at -1.5 V could be associated with the inaccurate consideration of a 100 % deposition efficiency process. This loss in efficiency at more cathodic applied potentials can be ascribed to the hydrogen evolution reaction (HER) that is usually found at lower deposition potentials [36]. In these cases, the current efficiency (σ) is then estimated by [36]

$$\sigma = \frac{j_{\text{ZnO}}}{(j_{\text{ZnO}} + j_{\text{HER}})},$$

where j_{ZnO} and j_{HER} are the current density values of the ZnO deposition process and the HER, respectively. To improve the accuracy of the current efficiency measurements, one should resort to more sophisticated methods [37–40]. Nevertheless, even when considering a 90 % drop of current efficiency at higher cathodic potentials [36], the thicker ZnO films would still be obtained for applied potentials of -1.5 V and temperatures of 80 °C (either at 0.01 or 0.1 M), thus making these values the optimum conditions for the growth of thicker ZnO films.

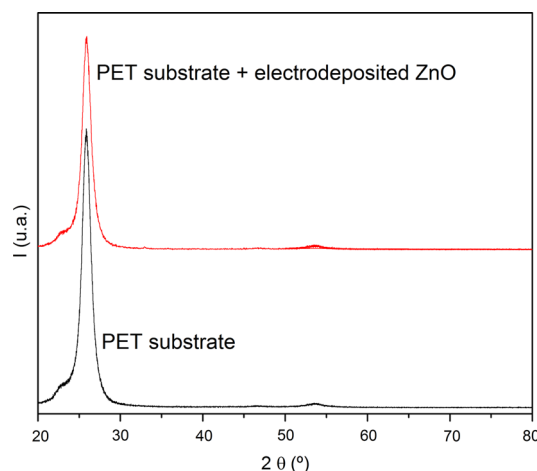


Figure 5 XRD spectra of a PET substrate (*black line*) and a representative ZnO electrodeposited thin film on top of a PET substrate (*red line*).

Crystallographic structure

Figure 5 shows the XRD spectra of the substrate prior to the deposition process and of a representative ZnO thin film sample (-1.1 V with a concentration of 0.01 M at 80 °C). We can observe that the obtained spectra are very similar, thus showing only the presence of the crystallographic peaks of the substrate. Such spectrum suggests that the electrodeposition of ZnO on PET/ITO flexible substrates does not produce crystalline structures but rather an amorphous (or nanocrystalline) phase, for the studied parameters in this work. Nevertheless, further analysis of the crystallographic structure of the deposited films should be performed using grazing incidence XRD measurements and/or selected area electron diffraction techniques, to better understand the overall crystallographic structure and/or the possible formation of nanocrystalline phases.

Morphology: deposition at room temperature

Figure 6 shows the SEM images of the deposited samples using 0.1 M of ZNH, illustrating the different surface morphologies obtained when varying the applied potential: -1.0 V (a_1 and a_2), -1.1 V (b_1 and b_2), and -1.5 V (c_1 and c_2). All samples revealed traces of Zn and O on the EDS spectra (not shown), with increasing relative counts of Zn and O for lower potential, indicating an increase of the deposition rate

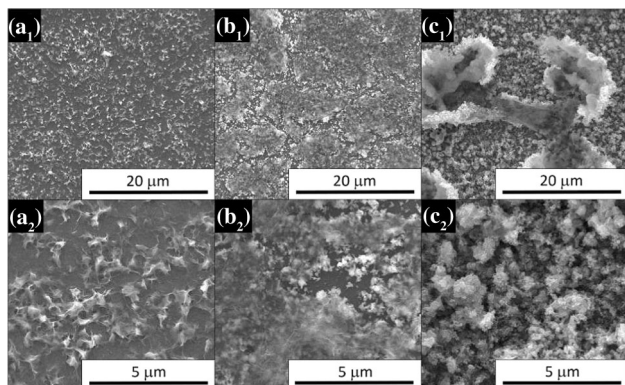


Figure 6 SEM images of electrodeposited ZnO, at different scales, at room temperature, for 0.1 M of ZNH with applied potentials of (**a**₁ and **a**₂) -1.0 V, (**b**₁ and **b**₂) -1.1 V, and (**c**₁ and **c**₂) -1.5 V.

at more negative applied potentials. The deposited films' morphology revealed the nucleation of ZnO nanostructures in the substrate surface for the highest (-1.0 V) potential, without the formation of a continuous film. As shown in Figs. 6a₁, b₁, c₁, the electrodeposition of ZnO tends to form clusters of nanostructures without forming a continuous film. This means that such deposition favors an island-like growth, creating areas with higher ZnO density. In the final stage of the deposition, the ZnO forms almost flat zones at the top of the islands, as seen in Fig. 6c₁.

When changing the electrolyte concentration to a tenth of the previous amount, the prepared samples revealed a much different morphology, displaying now planar *microramifications* of very small height, especially when applying a potential of -1.0 or -1.1 V (Fig. 7a, b). Furthermore, we can verify that the deposition at room temperature with 0.01 M and under -1.5 V has two morphologies (Fig. 7c): an initial deposition of *microflowers* followed by a top flat layer with *nanospheres* clustered on the surface. Such behavior can be related with the corresponding deposition current transient (Fig. 2d) and the deposited charge curves (Fig. 3d) where, as previously detailed, two distinct behaviors can be noticed. An initial one, during the first thousand seconds with high current values that progressively decrease and linear charge density transients, where ZnO *microflowers* are formed. Then, a second stage starts where the current remains constant at its minimum value, forming a flat ZnO surface with clustered *nanospheres*. The initially deposited ZnO *microflowers*

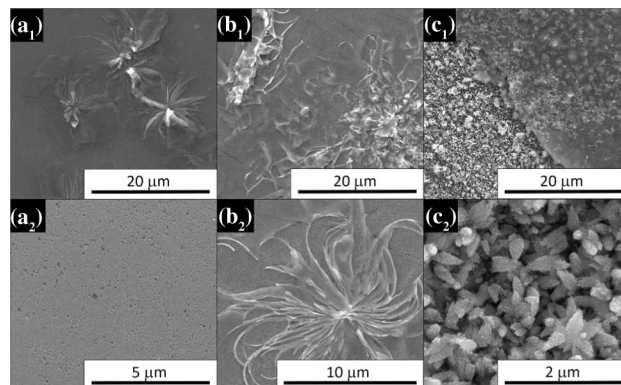


Figure 7 Electron microscopy of ZnO-deposited surface, at different scales, with an electrolyte of 0.01 M of ZNH at room temperature, with applied potentials of (**a**₁ and **a**₂) -1.0 V, (**b**₁ and **b**₂) -1.1 V, and (**c**₁ and **c**₂) -1.5 V.

have an effective deposition area much larger than the followed ZnO flat surface with small *nanospheres*. This can thus explain the large deposition currents measured during the first stage (Fig. 2d), corresponding to the formation of ZnO *microflowers*, and the subsequent drop in current, due to the final deposition of a flat ZnO surface.

Morphology: deposition at 80 °C

The obtained results for the electrodeposited samples with 0.1 M electrolyte at 80 °C are shown in Fig. 8 and can be compared with the ones deposited at room temperature (Fig. 6). One immediately notices a clear change in the samples morphology upon decreasing the applied potential to more negative values. At -1.0 V, ZnO nucleates in clustered nanostructures, which are absent at lower deposition potentials (Fig. 8a). At -1.1 V, ZnO forms localized *webs* that grow on top of each other, as seen in Fig. 8b₁, b₂. On the other hand, at -1.5 V, the formed nanostructures are much different, resembling *coral-like* structures of assembled particles (Fig. 8c). Thus the heating of the electrolyte provided a change in the ZnO nanostructures compared to the room temperature samples and to the different potentials applied at 80 °C.

Finally, we electrodeposited ZnO using an heated electrolyte at 80 °C with a concentration of 0.01 M. The produced samples (Fig. 9) revealed the nucleation of nanostructures similar to those previously presented in Fig. 8a, although with a lower density,

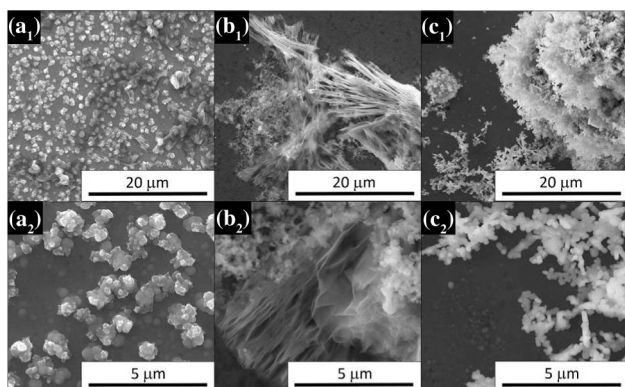


Figure 8 Electron microscope results for 0.1 M of ZNH solution at 80 °C, with deposition potentials of (a₁ and a₂) –1.0 V, (b₁ and b₂) –1.1 V, and (c₁ and c₂) –1.5 V.

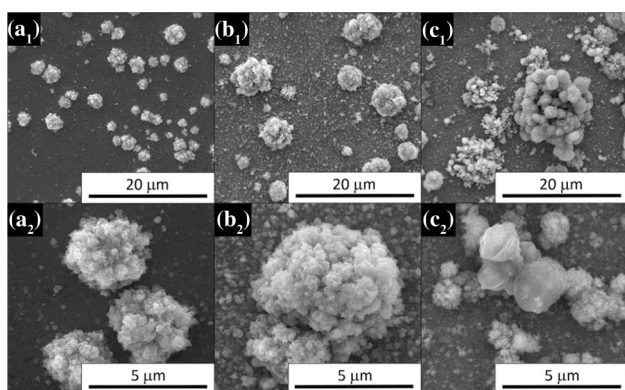


Figure 9 SEM images of ZnO-deposited thin films, at different scales, at 80 °C, for 0.01 M of ZNH with deposition potentials of (a₁ and a₂) –1.0 V, (b₁ and b₂) –1.1 V, and (c₁ and c₂) –1.5 V.

due to the lower concentration of the electrolyte. Differently from the 0.1 M concentration, all the applied potentials show the same type of ZnO nanostructures, with increasing dimensions for more negative potentials.

Conclusions

A thorough study was performed on the morphology of ZnO thin films electrodeposited on PET/ITO substrates upon varying the ZNH concentration, applied potential, and electrolyte temperature. The increase in the temperature of the electrolyte and ZNH concentration, along with the decrease of the applied negative potential, were found to increase the

deposition current and thus the total charge deposited. By varying the applied potential one can greatly change the morphology of the electrodeposited films. For 0.01 M of ZNH at 80 °C, the nanostructures increase in size when decreasing the applied potential to more negative values, maintaining the same shape. Also, in the specific case of 0.01 M, –1.5 V at RT, two distinct morphologies were observed by SEM and correlated with the two different regions exhibited by the current deposition transients, indicating the influence of the applied potential during deposition. All three parameters tend to change the films' morphology, as seen by SEM, allowing the exploration of different ZnO nanostructures for a wide range of purposes. Finally, the obtained results provided a better understanding of the deposition of ZnO nanostructures on flexible conducting substrates using electrochemical processes.

Acknowledgements

The authors acknowledge funding from FEDER and ON2 through project Norte-070124-FEDER-000070 and from FCT through the Associated Laboratory IN and project PTDC/CTM-NAN/122868/2010. JV acknowledges financial support through FSE/POPH. MPP is thankful to FCT for grant SFRH/BPD/84948/2012 supported by funding POPH/FSE. FF acknowledges financial support through Passaporte para o Empreendedorismo application number 2024 from IAPMEI/IP.

References

- [1] Wang ZL, Song J (2006) Piezoelectric nanogenerators based on zinc oxide nanowire arrays. *Science* 312(5771):242–246. doi:[10.1126/science.1124005](https://doi.org/10.1126/science.1124005)
- [2] Yang Y, Guo W, Pradel KC, Zhu G, Zhou Y, Zhang Y, Hu Y, Lin L, Wang ZL (2012) Pyroelectric nanogenerators for harvesting thermoelectric energy. *Nano Lett* 12(6):2833–2838. doi:[10.1021/nl3003039](https://doi.org/10.1021/nl3003039)
- [3] Bai P, Zhu G, Liu Y, Chen J, Jing Q, Yang W, Ma J, Zhang G, Wang ZL (2013) Cylindrical rotating triboelectric nanogenerator. *ACS Nano* 7(7):6361–6366. doi:[10.1021/nm402491y](https://doi.org/10.1021/nm402491y)
- [4] Nagaraju G, Ko YH, Yu JS (2015) Effect of diameter and height of electrochemically-deposited ZnO nanorod arrays on the performance of piezoelectric nanogenerators. *Mater Chem Phys* 149–150:393–399. doi:[10.1016/j.matchemphys.2014.10.034](https://doi.org/10.1016/j.matchemphys.2014.10.034)

- [5] Xu S, Qin Y, Xu C, Wei Y, Yang R, Wang ZL (2010) Self-powered nanowire devices. *Nat Nanotechnol* 5(5):366–373. doi:10.1038/nnano.2010.46
- [6] Janotti A, Van de Walle CG (2009) Fundamentals of zinc oxide as a semiconductor. *Rep Prog Phys* 72(12):126501. doi:10.1088/0034-4885/72/12/126501
- [7] Ikeda T (1990) Fundamentals of piezoelectricity. Oxford University Press, Oxford
- [8] Oliveira FF, Proenca MP, Araujo JP, Ventura J (in press) Output Potential of ZnO Nanowires: influence of Geometrical Parameters. *J Nanosci Nanotechnol*. doi:10.1166/jnn.2016.10729
- [9] Cataño FA, Gomez H, Dalchiele EA, Marotti RE (2014) Morphological and structural control of electrodeposited ZnO thin films and its influence on the photocatalytic degradation of methyl orange dye. *Int J Electrochem Sci* 9:534–548
- [10] Lu H, Deng K, Shi Z, Liu Q, Zhu G, Fan H, Li L (2014) Novel ZnO microflowers on nanorod arrays: local dissolution-driven growth and enhanced light harvesting in dye-sensitized solar cells. *Nanoscale Res Lett* 9:183. doi:10.1186/1556-276X-9-183
- [11] Wang ZL (2004) Zinc oxide nanostructures: growth, properties and applications. *J Phys Condens Matter* 16(25):R829. doi:10.1088/0953-8984/16/25/R01
- [12] Kumar PS, Maniam SM, Sundaramurthy J, Arokiaaraj J, Mangalaraj D, Rajarathnam D, Srinivasan MP, Jian LK (2012) Growth specificity of vertical ZnO nanorods on patterned seeded substrates through integrated chemical process. *Mater Chem Phys* 133(1):126–134. doi:10.1016/j.matchemphys.2011.12.076
- [13] Antohe VA, Gence L, Srivastava SK, Piroux L (2012) Template-free electrodeposition of highly oriented and aspect-ratio controlled ZnO hexagonal columnar arrays. *Nanotechnology* 23(25):255602. doi:10.1088/0957-4484/23/25/255602
- [14] Hou Q, Zhu L, Chen H, Liu H, Li W (2012) Growth of flower-like porous ZnO nanosheets by electrodeposition with $Zn_5(OH)_8(NO_3)_2 \cdot 2H_2O$ as precursor. *Electrochim Acta* 78(3):55–64. doi:10.1016/j.electacta.2012.05.113
- [15] Dunkel C, Wark M, Oekermann T, Ostermann R, Smarsly BM (2013) Electrodeposition of zinc oxide on transparent conducting metal oxide nanofibers and its performance in dye sensitized solar cells. *Electrochim Acta* 90:375–381. doi:10.1016/j.electacta.2012.12.048
- [16] Zarbska K, Kwiatkowski M, Gniadek M, Skompska M (2013) Electrodeposition of Zn(OH)₂, ZnO thin films and nanosheet-like Zn seed layers and influence of their morphology on the growth of ZnO nanorods. *Electrochim Acta* 98:255–262. doi:10.1016/j.electacta.2013.03.051
- [17] Matei E, Enculescu M, Preda N, Enculescu I (2012) ZnO morphological, structural and optical properties control by electrodeposition potential sweep rate. *Mater Chem Phys* 134(2–3):988–993. doi:10.1016/j.matchemphys.2012.03.101
- [18] Gomez JL, Tigli O (2012) Zinc oxide nanostructures: from growth to application. *J Mater Sci* 48(2):612–624. doi:10.1007/s10853-012-6938-5
- [19] Subannajui K, Güder F, Danhof J, Menzel A, Yang Y, Kirste L, Wang C, Cimalla V, Schwarz U, Zacharias M (2012) An advanced fabrication method of highly ordered ZnO nanowire arrays on silicon substrates by atomic layer deposition. *Nanotechnology* 23(23):235607. doi:10.1088/0957-4484/23/23/235607
- [20] Zhang H, Ma X, Xu J, Niu J, Yang D (2003) Arrays of ZnO nanowires fabricated by a simple chemical solution route. *Nanotechnology* 14(4):423. doi:10.1088/0957-4484/14/4/303
- [21] Znaidi L, Illia GS, Benyahia S, Sanchez C, Kanaev A (2003) Oriented ZnO thin films synthesis by sol gel process for laser application. *Thin Solid Films* 428(1–2):257–262. doi:10.1016/S0040-6090(02)01219-1
- [22] Gayen RN, Sarkar K, Hussain S, Bhar R, Pal AK (2011) ZnO films prepared by modified sol-gel technique. *Ind J Pure Appl Phys* 49(7):470–477
- [23] Bechelany M, Amin A, Brioude A, Cornu D, Miele P (2012) ZnO nanotubes by template-assisted sol-gel route. *J Nanoparticle Res* 14(8):980. doi:10.1007/s11051-012-0980-8
- [24] Wang ZL (2008) Self-powered nanotech. *Sci Am* 298:82–87. doi:10.1038/scientificamerican0108-82
- [25] Vaezi M, Sadrnezhad S (2007) Nanopowder synthesis of zinc oxide via sol-chemical processing. *Mater Des* 28(2):515–519. doi:10.1016/j.matdes.2005.08.016
- [26] Vergés MA, Mifsud A, Serna CJ (1990) Formation of rod-like zinc oxide microcrystals in homogeneous solutions. *J Chem Soc Faraday Trans* 86(6):959–963. doi:10.1039/ft9908600959
- [27] Vayssieres L, Keis K, Lindquist SE, Hagfeldt A (2001) Purpose-built anisotropic metal oxide material: 3D highly oriented microrod array of ZnO. *J Phys Chem B* 105(17):3350–3352. doi:10.1021/jp010026s
- [28] Baruah S, Dutta J (2009) Hydrothermal growth of ZnO nanostructures. *Sci Technol Adv Mater* 10(1):013001. doi:10.1088/1468-6996/10/1/013001
- [29] De Andrade Gomes M, Valerio MEG, Rey JFQ, Macedo ZS (2013) Comparative study of structural and optical properties of ZnO nanostructures prepared by three different aqueous solution methods. *Mater Chem Phys* 142(1):325–332. doi:10.1016/j.matchemphys.2013.07.024
- [30] Wellings J, Chaure N, Heavens S, Dharmadasa I (2008) Growth and characterisation of electrodeposited ZnO thin

- films. *Thin Solid Films* 516(12):3893–3898. doi:[10.1016/j.tsf.2007.07.156](https://doi.org/10.1016/j.tsf.2007.07.156)
- [31] Sousa CT, Leitao DC, Proenca MP, Ventura J, Pereira AM, Araujo JP (2014) Nanoporous alumina as templates for multifunctional applications. *Appl Phys Rev* 1(3):031102. doi:[10.1063/1.4893546](https://doi.org/10.1063/1.4893546)
- [32] Liu Z, Jin Z, Qiu J, Liu X, Wu W, Li W (2006) Preparation and characteristics of ordered porous ZnO films by a electrodeposition method using PS array templates. *Semicond Sci Technol* 21(1):60. doi:[10.1088/0268-1242/21/1/011](https://doi.org/10.1088/0268-1242/21/1/011)
- [33] Ehl RG, Ihde AJ (1954) Faraday's electrochemical laws and the determination of equivalent weights. *J Chem Educ* 31(5):226. doi:[10.1021/ed031p226](https://doi.org/10.1021/ed031p226)
- [34] Strong FC (1961) Faraday's laws in one equation. *J Chem Educ* 38(2):98. doi:[10.1021/ed038p98](https://doi.org/10.1021/ed038p98)
- [35] Bicelli LP, Bozzini B, Mele C, D'Urzo L (2008) A review of nanostructural aspects of metal electrodeposition. *Int J Electrochem Sci* 3:356–408
- [36] Proenca MP, Sousa CT, Ventura J, Vazquez M, Araujo JP (2012) Ni growth inside ordered arrays of alumina nanopores: enhancing the deposition rate. *Electrochim Acta* 72:215–221. doi:[10.1016/j.electacta.2012.04.036](https://doi.org/10.1016/j.electacta.2012.04.036)
- [37] Deligianni H, Romankiw LT (1993) In situ surface pH measurement during electrolysis using a rotating pH electrode. *IBM J Res Develop* 37(2):85–95. doi:[10.1147/rd.372.0085](https://doi.org/10.1147/rd.372.0085)
- [38] Allongue P, Cagnon L, Gomes C, Gündel A, Costa V (2004) Electrodeposition of Co and Ni/Au (111) ultrathin layers. Part I: nucleation and growth mechanisms from in situ STM. *Surf Sci* 557:41–56. doi:[10.1016/j.susc.2004.03.016](https://doi.org/10.1016/j.susc.2004.03.016)
- [39] Zafeiratos S, Paloukis FE, Neophytides SG (2004) Nickel electrodeposition on a gold polycrystalline foil: a combined voltammetric and photoelectron spectroscopy study. *J Phys Chem B* 108:1371–1379. doi:[10.1021/jp035804q](https://doi.org/10.1021/jp035804q)
- [40] Leistner K, Krause A, Fähler S, Schlörb H, Schultz L (2006) Electrode processes during Fe–Pt electrodeposition studied by electrochemical quartz crystal microbalance. *Electrochim Acta* 52:170–176. doi:[10.1016/j.electacta.2006.04.055](https://doi.org/10.1016/j.electacta.2006.04.055)